Waves filtering in heading controllers: impact on the power production of an energy ship

Giovanni Juin-Gauthier, Aurélien Babarit, Baptiste Elie, Olivier Kermorgant, Vincent Frémont

Waves filtering in heading controllers: impact on the power production of an energy ship ⋆

Giovanni Juin-Gauthier * **Aurélien Babarit** ** **Baptiste Elie** ***
Olivier Kermorgant **** **Vincent Frémont** ****

* *Nantes Université, École Centrale de Nantes, LS2N, UMR 6004, 44000 Nantes, France and Farwind Energy, France (e-mail: giovanni.juin-gauthier@farwind-energy.com).*
** *Nantes Université, École Centrale de Nantes, LHEEA, UMR 6598, 44000 Nantes, France (e-mail: aurelien.babarit@ec-nantes.fr)*
*** *Farwind Energy, France (e-mail: baptiste.elie@farwind-energy.com)*
**** *Nantes Université, École Centrale de Nantes, LS2N, UMR 6004, 44000 Nantes, France (e-mail: author@ec-nantes.fr)*

Abstract: This article investigates the impact on power production of an energy ship of two types of heading controllers. The first controller includes a filter which eliminates the wave-frequency dependent motion of the ship, while the other aims at compensating the effects of waves on the motion of the ship. The study is based on a numerical model of the energy ship which is presented in the paper. Results show that waves compensation reduces the generated power variation but increases rudder oscillations. In the opposite, the waves filtering controller allows for a slightly greater power production at the expense of greater power variations.

Keywords: Control applications in marine renewable energy, Modeling, identification, simulation, and control of marine systems, Guidance, navigation and control (GNC) of marine vessels

1. INTRODUCTION

To date, wind energy is exploited only on land and nearshore. In contrast, offshore wind energy in the high seas is left unexploited despite having - by far - the greatest potential (Liu et al., 2008). This is because it would be challenging to deploy wind turbines far from shore, since as pointed out by Martinez and Iglesias (2022), connection, installation and maintenance costs increase significantly as distance to coast and water depth increase.

An alternative approach to harvest this energy is the energy ship, which was patented by Salomon (1982) and first investigated by Platzer and Sarigul-Klijn (2009). An energy ship is a wind-propelled ship equipped with hydrokinetic turbines. It can thus convert wind energy to electricity through its motion. The electricity can then be directly stored in batteries or transformed into hydrogen or Power-to-X fuels as proposed by Kim and Park (2010).

A detailed design of an energy ship has been proposed by Babarit et al. (2020). This design has the particularity of using Flettner rotors for wind propulsion. A similar design is shown in Figure 1. This choice was motivated by the high propulsive power of this type of sails relative to their surface (Lu and Ringsberg, 2020).

Fig. 1. Artist view of the Farwind Energy energy ship

In order to be economically viable, such an energy production system shall have a small number of crew members or even no crew members at all (autonomous ship). An important feature to reach this aim is the implementation of a heading controller, which, given an heading set point will control the rudders angle of the ship to reach this set point. Controllers that have been proposed for sailing ships include the Proportional-Integral-Derivative (PID) controllers (Tranzatto et al., 2015), model based controllers (Zhou et al. (2020)) or Fuzzy controllers (Abril et al., 1997), to name a few. According to Fossen and Perez (2009), most of modern heading controllers include waves filtering, which reduce the effects of waves in the input of the controller on the motion of the ship. However, it is also pointed out that in some cases it might be necessary or preferable not to filter the wave frequency motion of the ship and to try to compensate the oscillatory motion

⋆ This work was partially supported by the French Agence Nationale de la Recherche Technologique (ANRT).

induced by the waves. This article aims to give a first insight into the impact of the controller on the energy production of the considered ship. To do so, two controllers are compared. Both are based on a PID with Feed-Forward (FF), taking into account the wind, lift and drag forces from the elements of the ship. One of them also includes a wave compensation scheme in the FF term, while the other will get its inputs filtered to eliminate the waves induced motion of the ship. The paper is organised as follows: in Section 2 we introduce the model of the energy ship. Section 3 details the two controllers. Finally, Section 4 illustrates the behaviors in a simulation environment and highlights the differences between the controllers.

2. ENERGY SHIP MODEL

A dynamic model has been developed in order to predict the behaviour of the energy ship. For this purpose, the model calculates the ship's motion and energy production over time. The model parameters are the characteristics of the ship (dimensions, masses, appendages, thrusters, sails, ...) and of the control systems. The model has been partially validated against results of experiments carried out in late June 2021 on the Vioreau lake (France) (Juin-Gauthier et al., 2022).
The model is based on the classical planar, three degrees of freedom (DOF) (surge-sway-yaw) manoeuvrability model. Two frames of reference are used (Figure 2). The North-East-Down (NED) reference frame - which can be assumed inertial in the case of "flat Earth navigation" (Fossen, 2011) - is defined as the plane tangent to the surface of the Earth at the localisation of the ship. The body-fixed reference frame (G, x_b, y_b) is attached to the ship and follows its motion. The position of the ship in the NED reference frame is denoted $\eta = [X, Y, \psi]^T$. The velocities of the ship are denoted in the body frame as the vector $\nu = [u, v, \dot{\psi}]^T$.

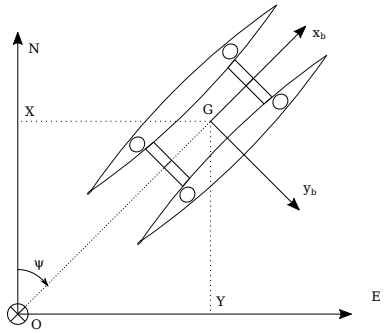

Fig. 2. Ship's reference frames

2.1 Kinematic and dynamic equations

According to Fossen (2011), the kinematic and dynamic equations for a manoeuvring three DOFs model are:

$$\dot{\eta} = \mathbf{J}(\eta)\nu \tag{1}$$

$$\mathbf{M}\dot{\nu} + (\mathbf{C}(\nu) + \mathbf{D}(\nu))\,\nu + \mu = \tau + \tau_{ex} \tag{2}$$

where :

- $\mathbf{J} = \begin{bmatrix} \cos\psi & -\sin\psi & 0 \\ \sin\psi & \cos\psi & 0 \\ 0 & 0 & 1 \end{bmatrix}$ is the rotation matrix between the body-fixed frame and the NED frame.
- $\mathbf{M} = \mathbf{M}_{\mathrm{RB}} + \mathbf{M}_{\mathrm{A}} = \begin{bmatrix} m & 0 & 0 \\ 0 & m & 0 \\ 0 & 0 & I_{zz} \end{bmatrix} + \begin{bmatrix} A_{11} & 0 & 0 \\ 0 & A_{22} & A_{26} \\ 0 & A_{62} & A_{66} \end{bmatrix}$ is the sum of the rigid body mass matrix ($\mathbf{M}_{\mathrm{RB}}$) and the added mass matrix at infinite frequency ($\mathbf{M}_{\mathrm{A}}$). m is the mass of the ship and I_{zz} is its yaw inertia. A_{11}, A_{22}, A_{26}, A_{62} and A_{66} are the added masses and added inertia of the ship due to water mass displacements (these terms have been obtained using the boundary element method software NEMOH.
- $$\mathbf{C} = \mathbf{C}_{\mathrm{RB}} + \mathbf{C}_{\mathrm{A}} = \begin{bmatrix} 0 & 0 & -mv \\ 0 & 0 & mu \\ mv & -mu & 0 \end{bmatrix} + \begin{bmatrix} 0 & 0 & -A_{22}v - A_{62}\dot{\psi} \\ 0 & 0 & A_{11}u \\ A_{22}v + A_{26}\dot{\psi} & -A_{11}u & 0 \end{bmatrix}$$ is the sum of the rigid body Coriolis matrix, $\mathbf{C}_{\mathrm{RB}}$, and the added mass Coriolis matrix at infinite frequency, $\mathbf{C}_{\mathrm{A}}$, at the ship's gravity centre G.
- $\mathbf{D}$ is the hydrodynamic damping matrix. Its coefficients have been computed using CFD.
- $\mu = \int_0^t \mathbf{K}(t-\tau)\delta\nu(\tau)d\tau$ is the convolution of the radiation Impulse Response Function (IRF), $\mathbf{K}$, of the ship, and its velocities variations $\delta\nu = \nu - \overline{\nu}$, with $\overline{\nu} = [\overline{u}, \overline{v}, 0]^T$ being the mean speed vector of the ship. This term corresponds to the fluid memory effect. It incorporates the energy of the radiated waves generated by the motion of the ship. $\mathbf{K}$ is defined from the frequency dependent damping and added masses matrices, $\mathbf{B}(\omega)$ and $\mathbf{M}_A(\omega)$ such that:
$$\mathbf{K}(t) = \frac{2}{\pi}\int_0^\infty \mathbf{B}(\omega)\cos(\omega t)d\omega - \frac{2}{\pi}\int_0^\infty (\mathbf{M}_A(\omega) - \mathbf{M}_A)\cos(\omega t)\mathbf{L}_s(\overline{\nu})d\omega$$
$\mathbf{L}_s(\overline{\nu}) = \begin{bmatrix} 0 & 0 & -\overline{v} \\ 0 & 0 & \overline{u} \\ 0 & 0 & 0 \end{bmatrix}$ is a selection matrix. $\mathbf{B}(\omega)$ and $\mathbf{M}_A(\omega)$ have been obtained using NEMOH.
- $\tau = [F_x, F_y, M_z]^T$ is the external forces vector applying to the ship. The detail of these forces is given in section 2.3.
- $\tau_{ex} = [F_{x,\mathrm{waves}}, F_{y,\mathrm{waves}}, M_{z,\mathrm{waves}}]^T$ is the combination of the Froude-Krylov forces vector and the diffraction forces vector applied on the ship by the waves (these forces have been obtained using NEMOH). These forces depend on the sea state, defined by the significant height of the waves H_s and the wave period T_s.

2.2 Energy ship design

The study uses an energy ship design developed by the company Farwind Energy. It is shown in Figure 1.

The Farwind Energy energy ship consists in an 80m long by 30m wide catamaran propelled by four Flettner rotors. Each rotor is 50m high and 5.5m in diameter. Two hydrokinetic turbines of 6m diameter are positioned underneath the hull. The ship is also equipped with two daggerboards of 21m^2 and two rudders of 6m^2.

2.3 Forces models

The systems that generate a force acting on the ship are the Flettner rotors, the hulls, the appendages, the rudders and the water turbines.

Hull : The hull force is broken down in two different forces : the total calm water resistance which represents the hull's resistance without drift and is defined in the longitudinal direction (G, x_b) of the ship, and the resistance due to the lift effect of the hull which induces both a lift effect in the (G, y_b) direction and an additional drag in the (G, x_b) direction. The calm water resistance F_T has been computed using CFD as presented by Insel and Molland (1992). It is taken into account in the dynamic model by linear interpolation in a table of forces depending on the Froude number $F_r = u/\sqrt{gL}$, where g is the gravity acceleration and L is the length of the ship. The lift effect of the hull depends on the leeway angle $\gamma = \arctan 2(v, u)$. The hull is assumed to behave as a foil with lift and drag coefficients. These coefficients C_l, C_d are estimated using the method described by Tillig and Ringsberg (2020) which are then integrated in the total forces of the hulls as follow:

$$F_{x,\text{hull}} = \underbrace{F_T(F_r)}_{\text{water resistance}} - \underbrace{0.5\rho_\text{w} A_\text{perp}(u^2+v^2)\left(C_l(\gamma)\sin\gamma - C_d\cos\gamma\right)}_{\text{added drag effect}}$$

$$F_{y,\text{hull}} = \underbrace{0.5\rho_\text{w} A_\text{perp}(u^2+v^2)\left(C_l(\gamma)\cos\gamma + C_d\sin\gamma\right)}_{\text{lift effect}}$$

where $F_{x,\text{hull}}$ is the total force along (G, x_b) and $F_{y,\text{hull}}$ along (G, y_b), ρ_w is the water density and A_perp is the ship's wetted surface projected in transverse direction.

Flettner rotors : The forces of the rotors are divided in two different forces. The drag force D, which is oriented along the wind flow direction and the lift force L, which is perpendicular to the wind flow direction, as shown in Figure 3. Those forces are defined as follow:

$$D = \frac{1}{2} C_D \rho_\text{air} V^2 A_R$$

$$L = \frac{1}{2} C_L \rho_\text{air} V^2 A_R$$

with C_L and C_D the lift and drag coefficients, A_R the projected surface of the rotor in the flow direction, V the apparent wind speed and ρ_air the density of air. Experimental campaigns have been conducted at different scales, by e.g Tillig and Ringsberg (2020) or Charrier (1979), to determine the lift and drag coefficients. It has been shown that these coefficients depend on the rotor's spin ratio $SR = \frac{\omega R_R}{V}$, where ω is the rotational speed of the rotor and R_R its radius. It corresponds to the ratio between the tangential speed of the rotor's surface and the apparent wind speed.

The results of Tillig and Rinsberg are implemented in the dynamic model, since the rotor size used in their study is comparable to that of the present study.

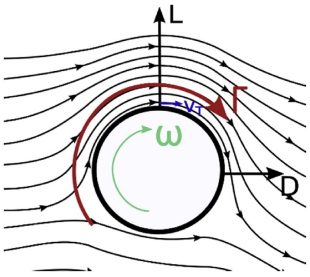

Fig. 3. Schematic of forces and wind flow around the rotor, Tillig and Ringsberg (2020)

The forces in the body-fixed frame are then :

$$F_{x,\text{rotor}} = D\cos\alpha - L\sin\alpha$$

$$F_{y,\text{rotor}} = D\sin\alpha + L\cos\alpha$$

where α is the apparent wind angle. The apparent wind is the sum of the true wind vector (wind observed by a stationary equipment) and the velocity vector of the ship.

Appendages and rudders : appendages are hydrofoils used to reduce the drift of the ship. Rudders are rotating hydrofoils that are used to control the heading of the ship. Both are taken into account using NACA0009 profiles. The lift $C_{l,\text{foil}}$ and drag $C_{d,\text{foil}}$ coefficients have been determined experimentally by Sheldahl and Klimas (1981). The forces are then :

$$F_{x,\text{foil}} = \frac{1}{2}\rho_\text{w} A_\text{foil} \overline{U}^2 \left(C_{d,\text{foil}}\cos\gamma - C_{l,\text{foil}}\sin\gamma\right)$$

$$F_{y,\text{foil}} = -\frac{1}{2}\rho_\text{w} A_\text{foil} \overline{U}^2 \left(C_{l,\text{foil}}\cos\gamma + C_{d,\text{foil}}\sin\gamma\right)$$

where ρ_w is the water density, A_foil is the surface of the profile, $\overline{U}$ is the total speed of the flow, including ship motion and γ is the angle of attack of the flow relative to the profile.

Hydrokinetic turbines : CFD simulations have been carried out on the hydrokinetic turbine's geometry to determine its drag coefficient C_T and power coefficient C_P for different tip speed ratios (TSR, which is the ratio between the tip blade speed and the flow speed) defined as follows: $TSR = \frac{D\Omega}{2u}$, with D the turbine diameter and Ω its rotational speed. The hydrokinetic turbine force is:

$$F_{x,\text{hydro}} = -\frac{1}{2}\rho_\text{w} C_T(TSR) u^2 A_\text{hydro}$$

$$F_{y,\text{hydro}} = 0$$

where A_hydro is the surface swept by the turbine blades. The mechanical power available on the turbine shaft P_hydro is given by :

$$P_\text{hydro} = \frac{1}{2}\rho_\text{w} C_P(TSR) u^3 A_\text{hydro} \tag{3}$$

The hydrokinetic turbines are attached to the hull with a lifting profile, which forces are described as the other hydrofoils.

Yaw momentum : the momentum, M_z relative to the z_b axis at the center of gravity of the ship G is computed for every elements. It is computed as follows :

$$M_z = \sum_i \left(F_{y,i}x_i - F_{x,i}y_i\right)$$

where i corresponds to the different elements of the ship listed above and where x_i and y_i are the coordinates of

the point of application of the force of element i in the ship-fixed frame.

3. HEADING CONTROL OF THE ENERGY SHIP

The aim of this paper is to study the effect of the heading control strategy on the production of an energy ship. Two types of heading controller are studied in this paper: a *PID-FF with waves filtering* and a *PID-FF with waves compensation*. The target heading of the ship is named ψ_{des}. The heading of the ship is controlled only by the rudders action. The rudder angle is denoted δ. The rudder angle is saturated both in amplitude and speed: δ cannot exceed $\pm$ 30° and $\dot{\delta}$ cannot exceed $\pm$ 3°/s. These values are representative of ships of size comparable to that of the ship of the present study.

3.1 PID corrector

At first, to reach and maintain ψ_{des}, a target yaw acceleration is defined. We rely on a PID controller that outputs an angular acceleration target $\ddot{\psi}_t$:

$$\ddot{\psi}_{\text{t}} = \ddot{\psi}_{\text{des}} + k_1(\dot{\psi}_{\text{des}} - \dot{\psi}) + k_2(\psi_{\text{des}} - \psi) + k3 \int_0^t (\psi_{\text{des}} - \psi) d\tau \tag{4}$$

In practice, $k_1 = 1$, $k_2 = 1/8$ and $k_3 = 0.005$ have proven to be satisfying values in term of stability, speed and overshoot performances.
To reach the angular acceleration target $\ddot{\psi}_{\text{t}}$ a momentum $M_{z,\text{t}} = (I_{zz} + A_{66})\ddot{\psi}_{\text{t}}$ must be applied at the centre of gravity of the ship.

3.2 FF with waves filtering

Let us assume that a measure (respectively an estimation) of the ship's positions vector η and velocities ν (respectively $\hat{\eta}$ and $\hat{\nu}$) is known. This measurements are then filtered with a notch filter cascaded with a low pass filter to eliminate the waves induced motion of the ship, as suggested by Fossen (2011). Then, it is possible to calculate the momentum of the different elements of the ship at the centre of gravity, excluding the rudders, using the equations presented in section 2.3. This momentum is called $M_{z,\text{FF}}$ and corresponds to the FF term.

$$M_{z,\text{FF}} = \sum_i (F_{y,i}(\hat{\eta}, \hat{\nu})x_i - F_{x,i}(\hat{\eta}, \hat{\nu})y_i) \tag{5}$$

where $i \in$ [hull, rotor, appendages, hydro].

3.3 FF with waves compensation

In the case of the FF with waves compensation, it is assumed that the states of the ship are also estimated or measured. They are denoted $\hat{\eta}$ and $\hat{\nu}$. It is also assumed that the sea state has been estimated. The significant wave height and wave period are denoted $\hat{H}_s$ and $\hat{T}_s$. Note that according to Komoriyama et al. (2023), the sea state can be estimated from the measurements of the motion of the ship. The FF term is then computed with the following equation:

$$M_{z,\text{FF}} = \sum_i (F_{y,i}(\hat{\eta}, \hat{\nu})x_i - F_{x,i}(\hat{\eta}, \hat{\nu})y_i) + M_{z,\text{waves}}(\hat{H}_s, \hat{T}_s) - \mu_z(\hat{\eta}, \hat{\nu}) \tag{6}$$

where $i \in$ [hull, rotor, appendages, hydro], $M_{z,\text{waves}}$ is the wave excitation moment and μ_z is the radiation moment.

3.4 PID-FF controller

The yaw momentum that the rudders must generate for the total momentum M_z to be equal to $M_{z,\text{t}}$ is then:

$$M_{z,\text{rudders,t}} = M_{z,\text{t}} - M_{z,\text{FF}}$$

Using an optimization method it is finally possible to find the optimal rudder angle δ_{opt} such that:

$$\delta_{\text{opt}} = \min_{\substack{\delta \\ |\delta|<\delta_{\max} \\ |\dot{\delta}|<\dot{\delta}_{\max}}} (M_{z,\text{rudders,t}} - M_{z,\text{rudders}}(\delta))^2 \tag{7}$$

where $\delta_{\max}$ and $\dot{\delta}_{\max}$ are the maximum rudder angle and angular velocity.

In figure 4, a block diagram of the controllers summarizes their architecture.

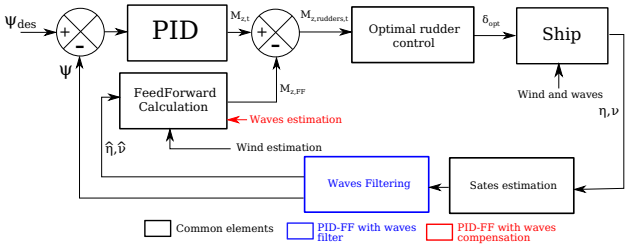

Fig. 4. Block diagram of the controllers

4. SIMULATION

We now illustrate the two controllers in a dynamic simulation. First, the simulation parameters are detailed. We then compare the induced behaviors depending on the FF term and the filtering of the wave frequency motion of the ship.

4.1 Simulation parameters

To investigate the performance of both controllers, simulations of the energy ship with the two different controllers in identical environmental conditions were carried out.

Constant heading setpoint The considered scenario is that of energy production. We assume that the ship has already reached its production zone and is now tracking a constant heading setpoint ψ_{des}, chosen to maximize energy production. Consequently, $\ddot{\psi}_{\text{des}} = \dot{\psi}_{\text{des}} = 0$. Without loss of generality it is assumed that the ship should sail towards North, corresponding to $\psi_{\text{des}} = 0°$ in the NED frame.

Environmental conditions The wind is supposed to be constant both in speed and direction.

- Wind speed: 10.5 m/s
- Wind angle: 270° (wind blowing from West to East)

The waves are supposed to be regular (i.e. the spectrum consists in only one frequency) and are coming from the same direction as the wind.

- Significant wave height (H_s): 1.4 m
- Wave period (T_s): 10 seconds
- Wave direction in NED frame: 90°

Note that those values correspond to mean values for measurements carried out by Lemessy et al. (2021) during a 10 years span in the Caribbean Sea, which is a possible deployment area for an energy ship.

Control parameters In this scenario the rotors are supposed to rotate at a constant speed $\omega_i = 130$ RPM $\forall i \in [|1, 4|]$.
Energy production can be tuned through the rotational speed of the hydrokinetic turbines. It is defined from the TSR that maximises the efficiency of the turbine $\frac{C_P(TSR)}{C_T(TSR)}$. In the scenario, $TSR_i = 3.1\ \forall i \in [|1, 2|]$.

Finally, the rudder angle is assumed to have the following limits in (7) : $\delta_{\max} = 30°$ and $\dot{\delta}_{\max} = 3°/s$.

4.2 Simulation results

As we use a constant heading setpoint and the waves are periodic, the simulation is run during 100 seconds. This corresponds to 10 waves. As we will see, the behavior is unchanged for the whole duration of the simulation. The time step was set to 0.1 seconds so as to properly compute the radiation term μ.

Figure 5 and 6 present a comparison of the results obtained with the two controllers. Results obtained with the PID-FF with waves filtering are plotted in blue (Waves filt.) and results obtained with PID-FF with waves compensation are plotted in red (Waves comp.). Figure 5 shows the forward speed of the ship, its yaw angle and the rudder angle for the two controllers. Figure 6 shows the data for one of the hydrokinetic turbines. That data include the generated power normalized by the mean power generated with the PID-FF with waves filtering controller, the rotational speed and the torque generated by the turbine (also normalized with the mean values obtained with the PID-FF with waves filtering controller).

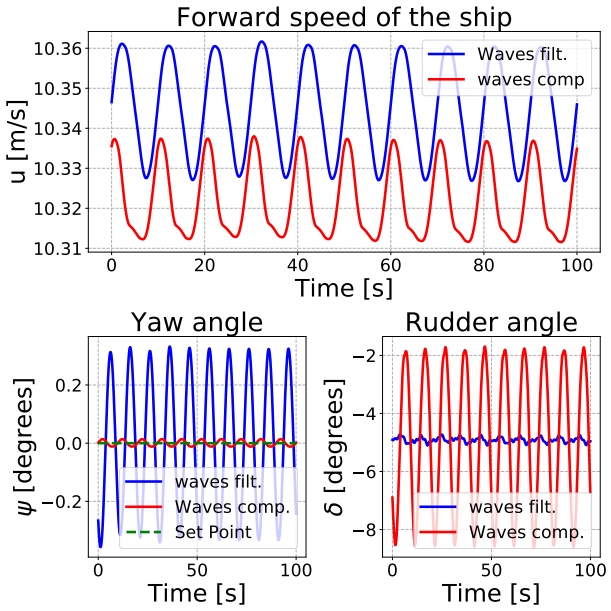

Fig. 5. Forward speed (top), yaw angle (bottom left) and rudder angle (bottom right) for the two controllers

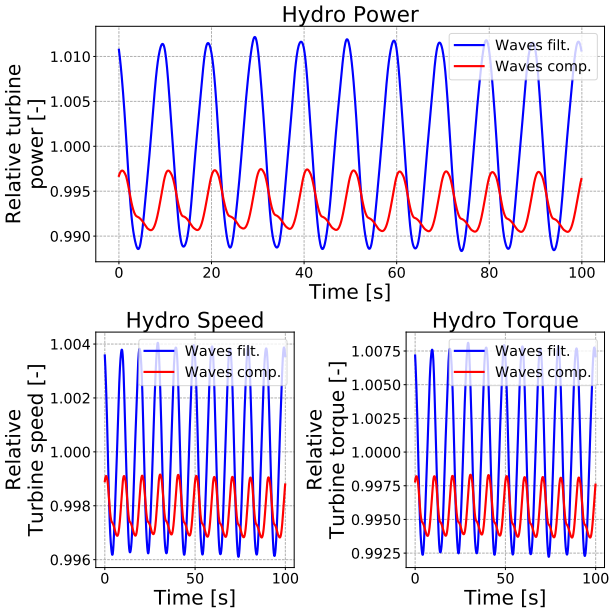

Fig. 6. Relative hydrokinetic turbines characteristics

5. DISCUSSION

It can be seen that the different controllers have little impact on the motion of the ship. As expected the yaw angle of the ship is closer to the set point with the PID-FF with waves compensation, however at the cost of greater amplitude of oscillations for the rudders angle. As a consequence the rudders generate more drag with this controller which is not compensated by the drag reduction obtained on the hull. The ship forward speed is consequently slightly greater with the PID-FF with waves filtering controller. Moreover, recalling that the power generated by the hydrokinetic turbines is proportional to the cube of the forward speed (see Equation 3), the mean power generated by the ship with the PID-FF with waves filtering controller is slightly greater than for the PID-FF with waves compensation. However, the power variation is also greater due to greater speed variations.

Figure 7 highlights the main differences between the two controllers, in terms of power generation and boat behavior. In particular, compensating the waves reduces by more than 240% the amplitude of the power fluctuations. This could be an interesting feature for an energy ship operator, since power variation may deteriorate prematurely the power conversion system. This comes at a negligible cost of a reduction of mean power output by approximately 0.7%. At the same time, relative to the power produced, this gives approximately a variation of 0.6% for the controller with wave compensation and 2% with waves filtering, which remains small in both cases

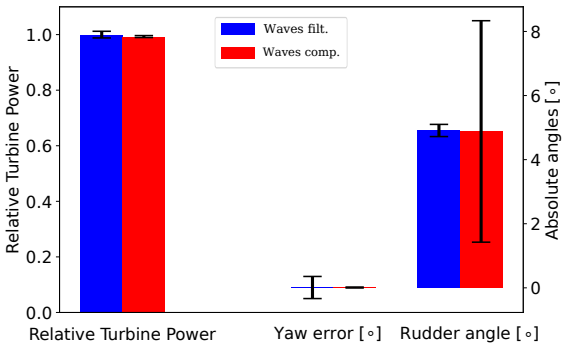

Fig. 7. Comparison of the power (left scale), yaw error and rudder angle (right scale) variations due to the type of controller

under these simulation conditions. This comes from the better overall yaw tracking (center bars in Fig. 7), due to a higher use of the rudder (right bars). In bigger waves, the dimensions of the rudders, as well as their dynamic could limit the compensation effect. If the rudder angle is saturated because of its speed, it may lead to an increasing heading error and even instability. If such a controller is implemented it would be necessary to set a sea state limitation beyond which the controller must be switched to another controller which filters the waves effects.

6. CONCLUSION

Waves filtering is often recommended when designing a marine heading controller, since it can reduce rudders oscillations and as a consequence can reduce the fatigue of their actuators. However, for new types of ships, such as the energy ship whose objectives are not the same as traditional ships, it is necessary to revisit this judgement. In this paper two types of controllers have been presented, differing in their capability to compensate for waves effects. Results show that trying to compensate for the waves effects reduce the amplitude of the power production variations, at cost of a slight reduction of the mean power production and of more solicitation of the rudders. As a consequence, the result of this study does not provide a clear answer to which approach is the best. It seems that preserving the rudders actuators may lead to a deterioration of the energy conversion system and at the opposite, preserving the energy conversion system may lead to a deterioration of the rudders actuators and to less energy production overall. A fatigue study of the different subsystems could clarify which one can be more solicited and give a clearer answer to the question. To complete our study, it would be appropriate to test these controllers on stronger sea states encountered in the Caribbean Sea in order to check whether the conclusions obtained remain valid.

REFERENCES

Abril, J., Salom, J., and Calvo, O. (1997). Fuzzy control of a sailboat. *International Journal of Approximate Reasoning*, 16(3-4), 359–375.

Babarit, A., Clodic, G., Delvoye, S., and Gilloteaux, J.C. (2020). Exploitation of the far-offshore wind energy resource by fleets of energy ships – Part 1: Energy ship design and performance. *Wind Energy Science*, 5(3), 839–853.

Charrier, B. (1979). *Etude théorique et expérimentale de l'effet Magnus destiné à la propulsion éolienne de navires*. PhD Thesis, Paris VI.

Fossen, T.I. (2011). *Handbook of Marine Craft Hydrodynamics and Motion Control*. Wiley, 1 edition.

Fossen, T.I. and Perez, T. (2009). Kalman filtering for positioning and heading control of ships and offshore rigs. *IEEE Control Systems*, 29(6), 32–46.

Insel, M. and Molland, A. (1992). An investigation into the resistance components of high speed displacement catamarans. *Trans. RINA*, 134, 1–20.

Juin-Gauthier, G., Elie, B., Kermorgant, O., Babarit, A., and Frémont, V. (2022). Experimental validation of a dynamic model of energy ships. In *25ème Congrès Français de Mécanique*, 80–90. CFM 2022.

Kim, J. and Park, C. (2010). Wind power generation with a parawing on ships, a proposal. *Energy*, 35(3), 1425–1432.

Komoriyama, Y., Iijima, K., Tatsumi, A., and Fujikubo, M. (2023). Identification of wave profiles encountered by a ship with no forward speed using Kalman filter technique and validation by tank tests - long-crested irregular wave case -. *Ocean Engineering*, 271, 113627.

Lemessy, K.G., Manohar, K., and Adeyanju, A. (2021). Analysis of the Caribbean wave climate for wave energy harvesting. *IET Renewable Power Generation*, 15(14), 3409–3423.

Liu, W.T., Tang, W., and Xie, X. (2008). Wind power distribution over the ocean. *Geophysical Research Letters*, 35(13), L13808.

Lu, R. and Ringsberg, J.W. (2020). Ship energy performance study of three wind-assisted ship propulsion technologies including a parametric study of the Flettner rotor technology. *Ships and Offshore Structures*, 15(3), 249–258.

Martinez, A. and Iglesias, G. (2022). Mapping of the levelised cost of energy for floating offshore wind in the European Atlantic. *Renewable and Sustainable Energy Reviews*, 154, 111889.

Platzer, M. and Sarigul-Klijn, N. (2009). A Novel Approach to Extract Power From Free-Flowing Water and High Altitude Jet Streams. In *ASME 2009 3rd International Conference on Energy Sustainability, Volume 1*, 493–499. ASMEDC, San Francisco, California, USA.

Salomon, R.E. (1982). Process of converting wind energy to elemental hydrogen and apparatus therefor.

Sheldahl, R.E. and Klimas, P.C. (1981). Aerodynamic characteristics of seven symmetrical airfoil sections through 180-degree angle of attack for use in aerodynamic analysis of vertical axis wind turbines. Technical Report SAND-80-2114, 6548367.

Tillig, F. and Ringsberg, J.W. (2020). Design, operation and analysis of wind-assisted cargo ships. *Ocean Engineering*, 211, 107603.

Tranzatto, M., Liniger, A., Grammatico, S., and Landi, A. (2015). The debut of Aeolus, the autonomous model sailboat of ETH Zurich. In *OCEANS 2015 - Genova*, 1–6. IEEE, Genova, Italy.

Zhou, X., Wu, Y., and Huang, J. (2020). MPC-based path tracking control method for USV. In *2020 Chinese Automation Congress (CAC)*, 1669–1673. IEEE, Shanghai, China.

.